Acta Oceanol. Sin., 2017, Vol. 36, No. 3, P. 26–36
DOI: 10.1007/s13131-017-1039-6
http://www.hyxb.org.cn
E-mail: hyxbe@263.net

The temporal and spatial variations in the Pacific wind and wave fields for the period 2002–2011

XU Yao[1, 2], BI Fan[1, 3, 4], SONG Jinbao[1, 5*], HE Hailun[6]

[1] Key Laboratory of Ocean Circulation and Waves, Institute of Oceanology, Chinese Academy of Sciences, Qingdao 266071, China

[2] University of Chinese Academy of Sciences, Beijing 100049, China

[3] North China Sea Marine Forecasting Center of State Oceanic Administration, Qingdao 266061, China

[4] Shandong Provincial Key Laboratory of Marine Ecological Environment and Disaster Prevention and Mitigation, Qingdao 266061, China

[5] Ocean College, Zhejiang University, Hangzhou 310058, China

[6] State Key Laboratory of Satellite Ocean Environment Dynamics, Second Institute of Oceanography, State Oceanic Administration, Hangzhou 310012, China

Received 6 January 2016; accepted 28 March 2016

Abstract

The temporal and spatial variations in the wind and wave fields in the Pacific Ocean between 2002 and 2011 are analyzed using a third-generation wave model (WAVEWATCH III). The model performance for a significant wave height is validated using *in situ* buoy data. The results show that the wave model effectively hindcasts the significant wave height in the Pacific Ocean, but the errors are relatively large in the mid- and low-latitude regions. The spatial distributions and temporal variations in a wind speed and the significant wave height in the Pacific Ocean are then considered after dividing the Pacific Ocean into five regions, which show meridional differences and seasonal cycles. Regional mean values are used to give yearly average time series for each separate zone. The high latitude region in the Southern Hemisphere had a stronger significant wave height trend in the model results than regions at other latitudes. The sources and sinks of wave energy are then investigated. Their regional mean values are used to quantify variations in surface waves. Finally, the spectral analyses of the daily mean wind speeds and the significant wave heights are obtained. The significant wave height and the wind speed spectra are found to be connected in some ways but also show certain differences.

Key words: the Pacific Ocean, wind speed, significant wave height, temporal and spatial variations, WAVEWATCH III

Citation: Xu Yao, Bi Fan, Song Jinbao, He Hailun. 2017. The temporal and spatial variations in the Pacific wind and wave fields for the period 2002–2011. Acta Oceanologica Sinica, 36(3): 26–36, doi: 10.1007/s13131-017-1039-6

1 Introduction

Surface waves have a direct impact on oceanic and atmospheric boundary layer structures, and the variations in the surface waves are important in oceanic and atmospheric dynamics (He and Chen, 2011; Li et al., 2013; Song et al., 2015). Research on spatial and temporal variations in ocean waves aims at providing scientific information for use in a marine engineering design, developments in the oceans, transportation, and marine fisheries. Spatially and temporarily consistent ocean wave data can be obtained using numerical simulations. WAVEWATCH III (hereafter WW3), which is a third-generation wave model, was developed at NOAA/NCEP following the same principles as the WAM model. The WW3 offers a high degree of precision and is very stable, and has become widely used in practical marine forecasts (Bi et al., 2015; Mentaschi et al., 2015).

The temporal and spatial distributions of waves are closely related to the temporal and spatial distributions of wind. Pogarskii et al. (2012) simulated wave fields in the Indian Ocean for the period 1998–2009 using wind fields from NOAA/NCEP and a modified wind–wave model WAM. They divided the Indian Ocean into a number of zones and analyzed the wind and wave characteristics of various zones. The temporal and spatial variations in waves in the Pacific have also been investigated. Liu et al. (2002) identified the general characteristics of, and rules for, the wave fields in the northern Pacific all year round using marine meteorological data covering 46 a. Han et al. (2003) analyzed the spatial distributions and temporal variations in the northern and southern Pacific significant wave heights using the data from the Topex/Poseidon altimeter for 75 consecutive months. Zhou et al. (2009) established a WW3 wave hindcast for the northwestern Pacific Ocean driven by the QSCAT/NCEP wind fields for 2005, and they simulated and summarized the characteristics of the spatial and temporal distributions of the wind and waves in that region. Zheng et al. (2012) used ERA-40 wave data from the European Centre for Medium-Range Weather Forecasts to analyze the sea surface wind, wind wave, swell wave, and overall wave fields for the Pacific Ocean.

In previous studies in which Pacific Ocean wave simulations have been established, rather more attention has been paid to wave variations in small parts of the Pacific Ocean than to the

Foundation item: The National High Technology Research and Development Program (863 Program) of China under contract No. 2013AA122803; the National Natural Science Foundation of China under contract Nos 41506033, 41576013 and 41476021.
*Corresponding author, E-mail: songjb@zju.edu.cn

ocean as a whole (He and Xu, 2016). Few studies have focused on the simulations of the entire Pacific or on the comparisons of waves caused by different wind belts. Wind input and breaking output source terms have not previously been reported for the Pacific Ocean. Here, we perform hindcasts for waves in the Pacific Ocean between 2002 and 2011 using the latest version of WW3. The simulated results are validated using observations from the study area. We assess the spatial and temporal variations in both wind speed and significant wave height, and analyze the spectrum characteristics and trends in the time series. We then assess the distributions of wave fields in different zones of the Pacific, determining the zones according to the wind belts. The results show that both local wind belts and remote waves in some areas need to be taken into account when analyzing the wave climate.

We describe a model configuration and a forcing field in Section 2, and then validate model results in Section 3. The results are presented in Section 4, with subsections in which we describe the spatial distributions and temporal variations in the wind speed and the significant wave height, the sources and sinks of the wave energy, and the power spectrum analysis. Finally, our conclusions are presented in Section 5.

2 Model configuration

The WW3 calculates the evolution of the wavenumber-direction spectrum $F(k, \theta)$. The effects of currents on waves mean that the wavenumber-direction spectrum is not conserved when currents are taken into account (Longuet-Higgins and Stewart, 1961, 1962), but the wave action density spectrum $N(k, \theta) \equiv F(k, \theta)/\sigma$ is still satisfied. Therefore, the parameterization is for the wave action density spectrum in the actual calculations. The wave propagation is described by

$$\frac{\mathrm{D}N}{\mathrm{D}t} = \frac{S}{\sigma},$$

where $\mathrm{D}/\mathrm{D}t$ is the total derivative and S is the net effect of the sources and sinks on the wave number–direction spectrum the wavenumber-direction spectrum, as shown below:

$$S = S_{\mathrm{in}} + S_{\mathrm{nl}} + S_{\mathrm{ds}} + S_{\mathrm{xx}}.$$

In deep water, the net source term S is mainly determined by three terms, a wind–wave interaction term S_{in}, a nonlinear wave–wave interactions term S_{nl}, and a dissipation (white capping) term S_{ds}. Other terms are used to represent wave–bottom interactions, depth-induced breaking, triad wave–wave interactions, and other phenomena. The meanings of the other terms are given in the WW3 (Version 4.18) manual (Tolman et al., 2014). The wind–wave interaction term S_{in} and the dissipation term S_{ds} represent separate physical processes, but should be considered to be related in the wave model (Kalantzi et al., 2009). Several new input and dissipation term packages have been introduced in the latest version of WW3 (Version 4.18). Here, we use the default Tolman and Chalikov (1996) (with switch ST2) source term, which has been used in many other studies.

The computational domain of the numerical wave model was the globe, with a horizontal grid resolution of 0.5°. Water depths were extracted from the ETOPO2 data set. The main area on which this study was focused was the Pacific Ocean, from 75°N to 75°S and from 90°E to 60°W, as shown in Fig. 1. We set 36 directions with 10° interval and 25 frequencies, from 0.04 to 0.4 Hz, with an increment factor of 1.1. The model spin-up was set to 1

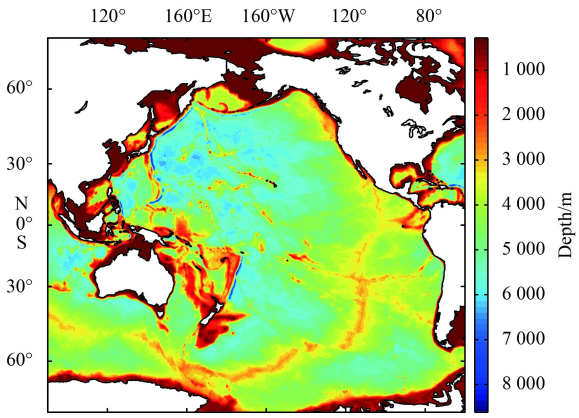

Fig. 1. Model domain and bathymetry.

month, and simulation results for the 10 a period of 2002–2011, were used for the analysis.

The wind field is the only force in the wave simulation. The wind field used in this study was obtained from a cross-calibrated multi-platform ocean surface wind velocity (CCMP) data set. This has a horizontal resolution of 0.25° and a time step of 6 h. The CCMP data are widely used in wave models (Zhang et al., 2011; Zhang et al., 2013; Zheng et al., 2013). Bi (2013) compared the CCMP wind field with SAR retrieved wind data, the European Centre for Medium-Range Weather Forecasts wind data provided by Envisat ASAR, and NDBC buoy observation wind data, and found that the CCMP wind data used in the wave model had a better average level of accuracy than the other data, and that the few points with larger errors were mainly at mid-to-high latitudes and near the coast.

3 Model validation

The model results were validated using buoy data provided by the NOAA National Data Buoy Center (NDBC). Buoys were selected where (1) the water depth was greater than 1 km, (2) the distance to shore was greater than 100 km, and (3) one- or two-dimensional wave spectra data were available. A total of 22 NDBC buoys in the Pacific Ocean were eligible, and their locations are shown in Fig. 2. Comparisons were made between the model results and the observations, mainly focusing on the correlation coefficient, root-mean-square error (RMSE), mean bias, and mean relative bias.

The significant wave heights determined using the model are plotted against the significant wave heights from the NDBC buoy observations for 2007 (Fig. 3). The corresponding statistical parameters are shown in Table 1. The correlation coefficients were all greater than 0.9, and the mean RMSE was 0.48 m. The validated results indicate that the WW3 generally simulated the significant wave height well. The buoy stations with negative deviations were concentrated at high northern latitudes, suggesting that the model probably underestimates waves at high latitudes. The RMSE was greater than 0.6 m and the mean relative bias was greater than 0.2 at five buoys, and these buoy stations are marked in red in Fig. 2. These buoys were concentrated at low latitudes, near the Hawaiian Islands. Despite the relatively poor ability of the model to simulate waves at low latitudes in the Pacific Ocean, the deviations were not significant and did not affect the overall simulation.

4 Results

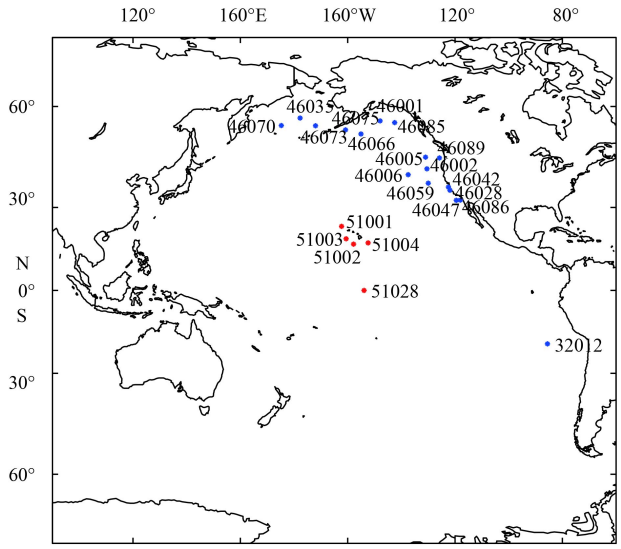

Fig. 2. Positions of the eligible buoys (points in red are buoys with larger simulated deviations).

4.1 *Spatial distributions and temporal variations of the wind speed*

We explored the multiscale temporal variations and spatial distributions of the wind speed field by constructing three types of wind speed field: (1) wind speed averaged over the entire decade; (2) January and July wind speeds averaged for each of 10 a and seasonal variations; and (3) the mean wind speed trend over the decade. The mean wind speeds were calculated from the absolute wind speed values.

The 10 a average wind speed distribution is shown in Fig. 4. There were clear variations in the spatial distribution of the wind speed field, and several extreme values were found. The distribution of the extreme wind speed values (corresponding to a mean wind speed contour line at 7 m/s, thus the major gyres) allowed the Pacific to be divided into five zones. The straight black lines in Fig. 4 indicate the boundaries of the zones. The latitude ranges covered by the zones are given in Table 2. Zones 3 (Z3) and 4 (Z4) were divided by a line drawn at 166°W.

The northernmost Zone 1 (Z1) was mostly to the north of 30°N. This area is controlled throughout the year by the Aleutian low. Z1 contains a large high-value central area in which the average wind speed was mostly greater than 8 m/s. The 10 a average wind speeds at low and mid-latitudes in Zone 2 (Z2) were 6–7 m/s. The center of Z2 was at about 15°N, near the Hawaiian Islands, where the average wind speed reached 8 m/s. It is worth mentioning that the Bashi Strait, in the west of Z2, also shows an area of high wind speed, while the eastern part, along the coast of North America, is clearly characterized by low wind speeds. Zone 3 (Z3) and Zone 4 (Z4) are both near the equator, but the wind speed distributions in the two areas are different. Z4, covering the eastern and central equatorial Pacific, is a high wind speed zone, with an average wind speed of greater than 6 m/s and the wind speeds in the center as high as 8 m/s. The wind speed distribution shows that in the west, Z3 can be further divided into two sections. The area closer to the equator and north of New Guinea

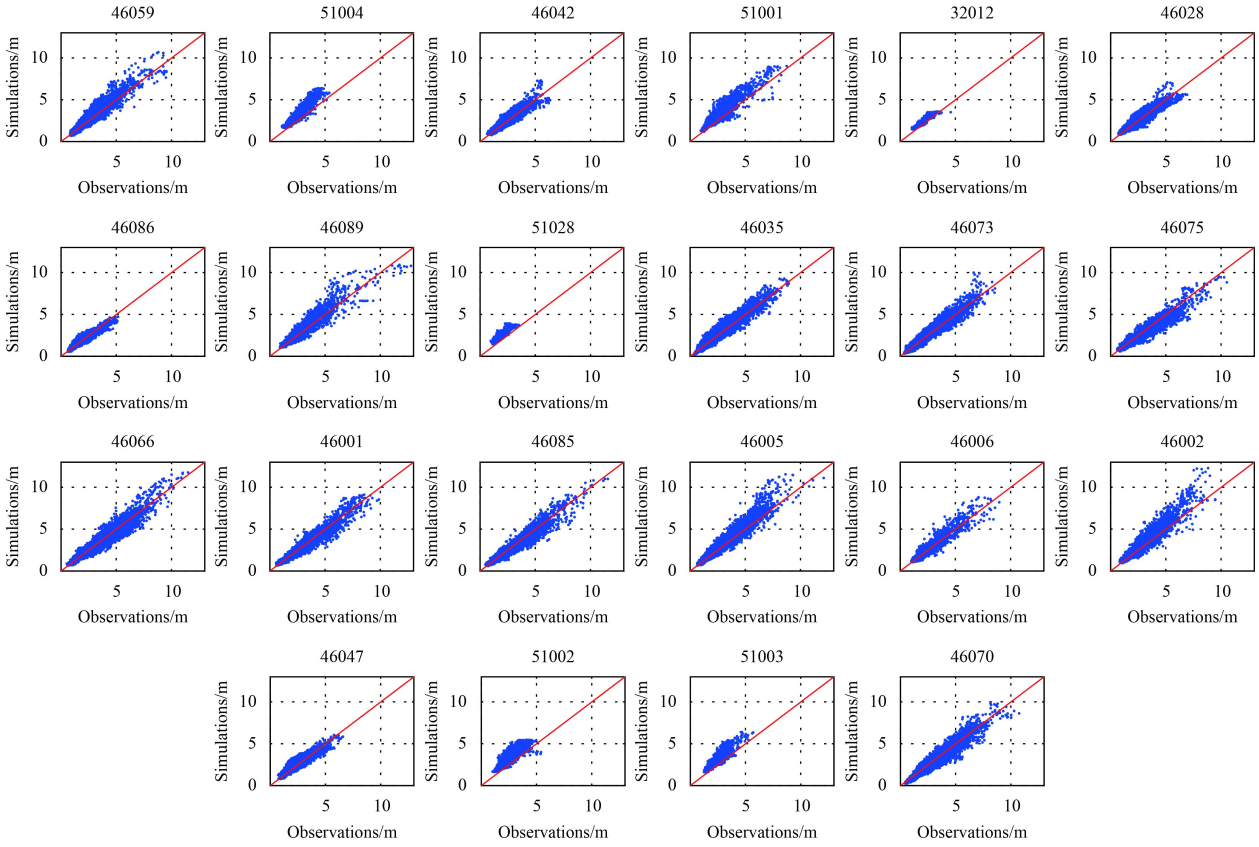

Fig. 3. Scatter plots of the significant wave heights determined by the model and by buoys operated by the NOAA National Data Buoy Center. The observed values are shown on the horizontal axes and the simulated values are shown on the vertical axes. The number above each subplot is the identification number of the buoy.

Table 1. Error statistics for the model results plotted against the observations made by the buoys

	Buoy No.	Water depth/m	Number of effective observations	Correlation coefficient	Mean bias/m	Mean relative bias	RMSE/m
1	46059	4 627.0	8 511	0.95	0.19	0.08	0.44
2	51004	5 230.0	6 840	0.94	0.60	0.26	0.67
3	46042	2 098.0	8 210	0.94	0.03	0.03	0.30
4	51001	3 430.0	8 290	0.94	0.58	0.26	0.68
5	32012	4 551.0	1 505	0.94	0.30	0.16	0.35
6	46028	1 158.2	8 671	0.93	–0.01	0.02	0.35
7	46086	1 828.8	7 794	0.94	–0.02	0.00	0.21
8	46089	2 289.0	2 578	0.94	0.22	0.08	0.63
9	51028	4 747.0	2 962	0.90	0.61	0.32	0.64
10	46035	3 658.0	5 827	0.96	0.12	0.05	0.46
11	46073	3 051.5	8 034	0.97	0.10	0.06	0.38
12	46075	2 487.0	5 943	0.96	–0.24	–0.06	0.50
13	46066	4 545.0	8 690	0.96	–0.03	0.00	0.44
14	46001	4 206.0	3 431	0.96	–0.11	–0.02	0.48
15	46085	3 736.3	5 535	0.97	–0.03	0.02	0.39
16	46005	2 853.0	8 684	0.96	0.21	0.08	0.49
17	46006	4 151.4	2 309	0.95	0.07	0.03	0.44
18	46002	3 444.0	7 693	0.95	0.31	0.11	0.58
19	46047	1 399.0	8 718	0.95	0.09	0.06	0.29
20	51002	5 029.2	8 682	0.92	0.65	0.27	0.73
21	51003	4 919.0	3 826	0.92	0.57	0.26	0.66
22	46070	3 804.0	8 705	0.96	–0.12	–0.06	0.43
Average value				0.945	0.19	0.09	0.48

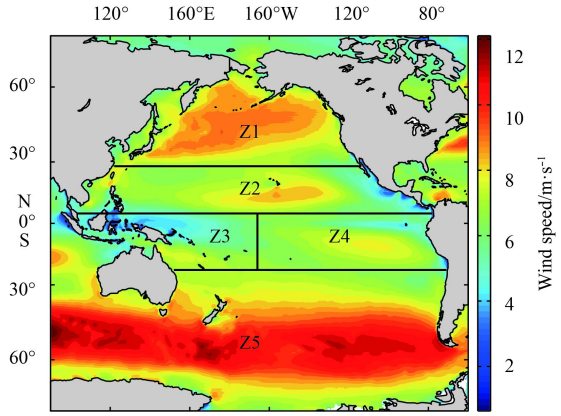

Fig. 4. Ten-year average wind speed distribution for the period 2002–2011.

Table 2. Latitude ranges of Zones 1–5 in the Pacific Ocean

Zone No.	Latitude range
1	28°–65°N
2	5°–28°N
3	23°S–5°N
4	23°S–5°N
5	65°–23°S

shows lower average wind speeds of less than 4 m/s, and the southern part, to the northeast of Australia, shows slightly higher average wind speeds of approximately 6 m/s. The wind speed distributions in the northern Pacific are almost consistent with the findings of Ma et al. (2013). Zone 5 (Z5) lies to the south of 23° S, and southern Pacific westerlies prevail in this area. The average wind speeds are 8–10 m/s in most parts of Z5, and the maximum wind speed is 12 m/s. The average wind speed is higher in Z5 than in the other zones, and this is related to an absence of land masses in this zone, meaning that the prevailing westerlies are largely unaffected by friction.

The average January wind speeds over the 10 a period are shown in Fig. 5a. The average wind speed was higher in Z1 than in the other zones. The wind speed reached 10 m/s in most parts of Z1, and the maximum was greater than 12 m/s. The high wind speed area in Z2 was longer and narrower in the average January distribution than in the 10 a average wind speed distribution. It bordered the Philippines in the west and 120° W in the east. The average wind speed was 10 m/s in the high wind speed area in the South China Sea. The wind speed was lower in Z3 than in the other zones, at only about 4 m/s, and the wind speed in Z4 was slightly higher, at about 7 m/s. Z5 had the second highest average wind speed, the average wind speed being 6 m/s in most parts of Z5 and 8 m/s between 40°S and 60°S.

The average July wind speeds over the 10 a study period are shown in Fig. 5b. The average wind speed was lower in Z1 (only 5–6 m/s) than in the other zones, and there was a local maximum wind speed in Z1 along the coast of California, United States. The average wind speed was a little higher in Z2 than in Z1. The high-wind area in Z2 was smaller in extent in the average July wind speed distribution than in the 10 a average wind speed distribution. The average wind speed in the eastern low-wind speed area of Z2 was only about 4 m/s, but the average wind speed in the center of the western high-wind speed area, in the South China Sea, reached 7–8 m/s. As for the 10 a average wind speed distribution, Z3 can be divided into two parts. The average wind speed north of New Guinea was only about 4 m/s, but the average wind speed northeast of Australia reached 9 m/s. The average wind speed in Z4 was about 8 m/s. The average wind speed in most parts of Z5 reached 10 m/s. The average wind speed in July was higher in Z5 than in the other zones, and this is related to the absence of land masses in this zone, meaning that the prevailing westerlies are relatively unaffected by friction.

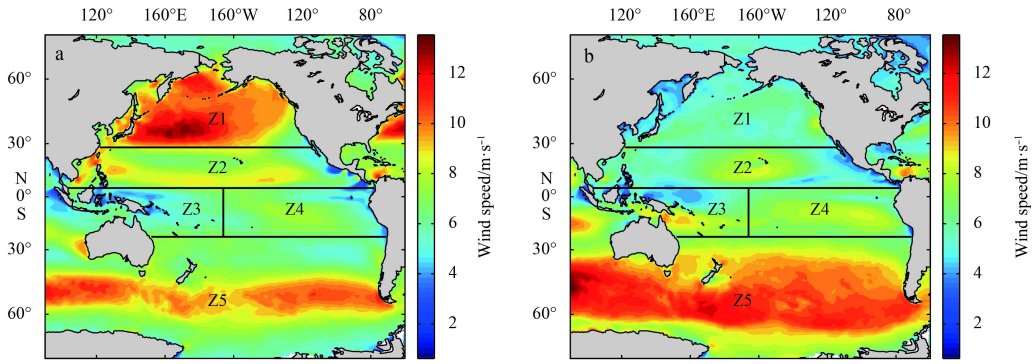

Fig. 5. Ten-year average wind speeds for January (a) and July (b).

We chose January and July to represent the boreal winter and summer, respectively. The difference between the January and July wind speeds averaged over 10 a was calculated to allow us to assess the seasonal variations in the average wind speed; these are shown in Fig. 6. Most of the differences were positive in the northern Pacific, meaning that, in most areas, the average wind speed was higher in the boreal winter than in the boreal summer. This was particularly the case in Z1, where the average wind speed was 6 m/s higher in January than in July. Two relatively wide areas of positive values were found, extending from the South China Sea in the western part of Z2 and from the coast of North America in the eastern part of Z2. The seasonal variations in both these areas were 4–5 m/s, so the wind speed was clearly much higher in the boreal winter than in the boreal summer. The seasonal variations were quite small in the southeastern part of Z1, along the coast of California, in the central part of Z2 (around 20°N), throughout Z4, and in the eastern part of Z5 (around 50°S). The difference was clearly negative in Z3, and the average wind speed there was 4 m/s higher in July than in January. The differences in most parts of Z5 were also negative, in other words the average wind speed was higher in July than in January. Even so, the strongest seasonal variations occurred in the northern Pacific. The average wind speed in the northern Pacific is much higher in the boreal winter (January) than in the boreal summer (July) because the boreal winter monsoon in the northern Pacific is strong and lasts a long time.

To attempt to understand the characteristics of the wind speed, we calculated time series for the yearly mean wind speeds averaged for each zone and for the whole Pacific Ocean, and these series are shown in Fig. 7. Consistent with the analyses described above, the highest yearly mean wind speeds were found for Z5, which had the highest average wind speed, and the next highest yearly mean wind speeds were for Z1, which also had a high average wind speed. The yearly mean wind speeds in the other zones decreased in the order Z2, Z4, and Z3. The interannual variabilities were relatively small for all the zones. The yearly mean wind speed for the entire Pacific increased at about 2.66 cm/s·a. Z4 contributed most of this increase, and the interannual variability here reached 4.98 cm/s. However, different trends were found for different zones. The interannual variabilities in Z1 and Z2 were less than 0.5 cm/s, but the rates of increase in Z3, Z4, and Z5 were higher. The yearly mean wind speed did not always increase, with a downward trend being found in some zones in some years.

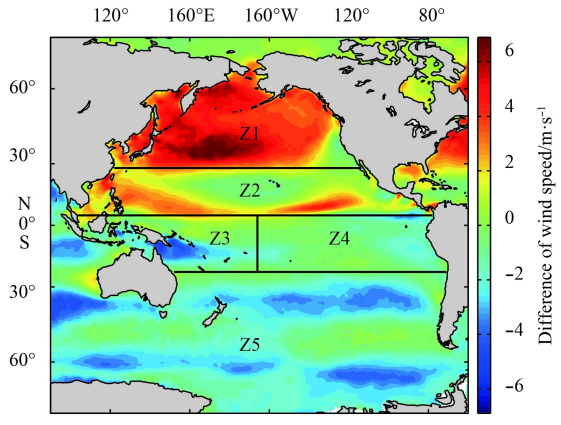

Fig. 6. Differences between the 10 a average wind speeds for January and July.

4.2 *Spatial distributions and temporal variations of significant wave height*

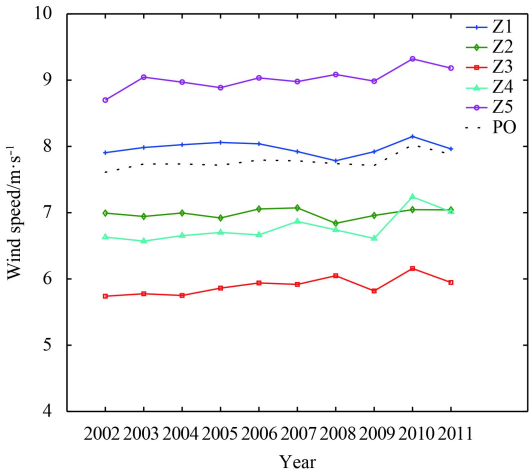

Fig. 7. Time series of the yearly mean wind speed averaged for each zone and for the entire Pacific Ocean (PO).

Like the wind speed field, the 10 a average significant wave height field shows a remarkable and sustained saddle-shaped distribution throughout the study area. High values were found at high latitudes in the north and the south, and low values were found at middle and low latitudes, as is shown in Fig. 8. The zone boundaries for the significant wave height field were somewhat shifted compared with the zone boundaries for the wind speed field. However, the differences in the boundaries were relatively

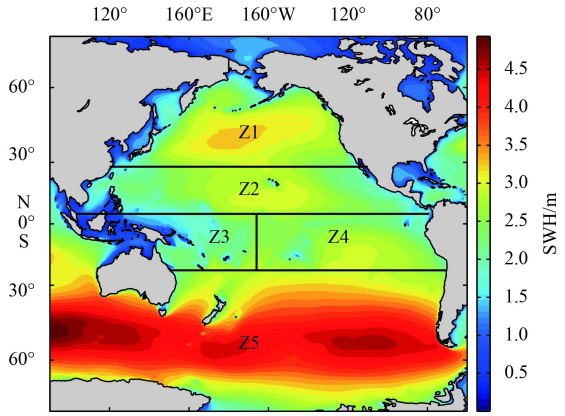

Fig. 8. Ten-year average significant wave height (SWH) distribution for the period 2002–2011.

small, so the Pacific Ocean could still be divided into five zones using the same lines as those used for the wind speed. The 10 a average significant wave height ranged from a minimum of less than 1 m in the boundary region to a maximum of greater than 4.5 m in Z5, in the south. The largest significant wave height was found for Z5, in the Southern Hemisphere, where the average was greater than 4 m and the maximum was greater than 4.5 m. The second largest significant wave height was found for Z1, at mid–high latitudes in the Northern Hemisphere, where the average was 2.5–3.5 m. The lowest significant wave height was found for Z3, in the western part of the equatorial area, where the average was less than 2 m.

The distribution of the average January significant wave height over the 10 a study period had a saddle-shaped distribution with higher values in the north and lower values in the south (Fig. 9a). The highest significant wave height was found for Z1, the second highest for Z2 and the third highest for Z5. The average July significant wave height in Z1 (in the northern Pacific) was about 1.5 m, and it gradually increased while moving south, reaching a maximum near 60°S in the southern Pacific in Z5 (Fig. 9b). The maximum average significant wave height was about 5.5 m, and this was found in the northern Pacific in January throughout the study period. In July (when higher values were found in the south and lower values in the north), the maximum value in the southern Pacific was only 5 m. The main causes of the differences in the distributions are the differences in land–sea distributions between the Northern and Southern Hemispheres, and cold waves being much stronger, more frequent, and longer lasting in the northern Pacific in January than elsewhere at other time.

The differences between the significant wave heights in January and July over the 10 a study period show very clear seasonal

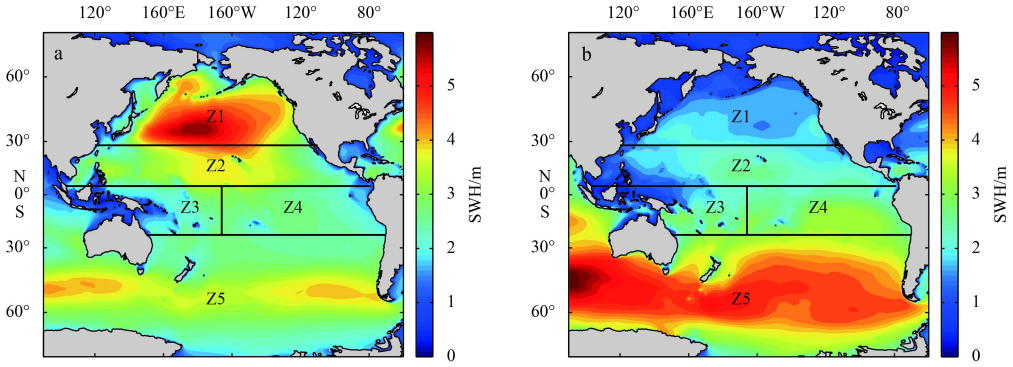

Fig. 9. Ten-year average significant wave heights for January (a) and July (b).

variations over the whole Pacific Ocean (Fig. 10). The seasonal variations in the significant wave heights were essentially the same as those in the wind speed. The significant wave height was clearly higher in July than in January over almost all of the southern Pacific. The difference between the significant wave heights in July and January in Z5 reached 2 m. The opposite pattern was found in the northern Pacific, the significant wave height being clearly higher in January than in July. The maximum difference was found in Z1, where the significant wave height was more than 3 m higher in January than in July. The seasonal differences were not as large in Z3 and Z4, which are near the equator.

Time series of the yearly mean significant wave height averages for each zone and for the whole Pacific Ocean are shown in Fig. 11. The average significant wave height was greater in Z5 than in the other zones, consistent with the results described above. The average significant wave heights were different in the different zones. For the entire Pacific, the average significant wave height increased at about 0.56 cm/a. We considered the zones separately, and found different increasing significant wave height trends in the different zones, and in some zones in some years we found downward trends. Over the whole study period, the significant wave heights decreased in Z1, Z2, and Z3 and in-

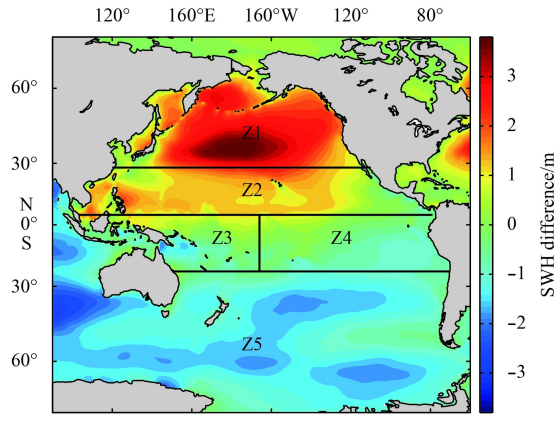

Fig. 10. Ten-year average significant wave height differences between January and July.

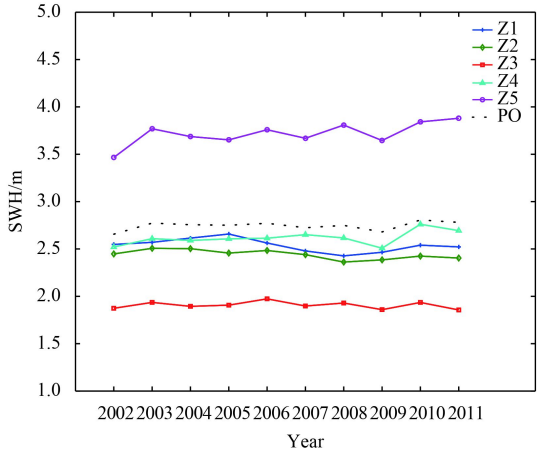

Fig. 11. Time series of the yearly mean significant wave height averages for the different zones and for the entire Pacific Ocean.

creased in Z4 and Z5. The absolute values of the interannual variations were less than 2 cm in every zone except Z5, in which the interannual variation was large. The absolute value in Z3, near the equator, was only 0.21 cm. It is worth noting that the largest interannual variation occurred in Z5. The significant wave height increased by 2.67 cm/a over the 10 a study period in Z5. Appendini et al. (2014) found that mean wave heights in the Caribbean Sea increased by 0.03 m/a, so interannual variations in the significant wave height of the magnitude we found cannot be ignored.

4.3 *Wave energy input and dissipation*

Besides the significant wave height field, we outputted the source terms from the model results to allow wave energy input and dissipation to be investigated at the same time. Like the wind speed and the significant wave height, the 10 a average wave energy input shows a saddle-shaped distribution, with high values in the north and the south and low values in the middle (shown in Fig. 12a). The Pacific Ocean was therefore divided into five zones along the lines described above. The maximum 10 a average wave energy input (>0.7 W/m^2) was found in Z5, in the southern Pacific. Large wave energy inputs (0.3–0.5 W/m^2) were also found at mid-to-high latitudes in the northern Pacific, in Z1. The wave energy inputs in Z2, Z3, and Z4 were relatively small. The dissipation source term in the wave model was negative. We used the absolute values of the dissipation source term to illustrate the distribution of the wave energy dissipation. The distribution of the wave energy dissipation was similar to the distribution of the wave energy input as shown in Fig. 12b. Zones with strong wave energy inputs (Z1 and Z5) also had strong wave energy dissipation, and the wave energy dissipation was relatively weak in Z2, Z3, and Z4.

The wave energy input and dissipation distributions in January and July averaged over 10 a show obvious seasonal variations at higher latitudes in the southern and northern Pacific, but not between 30°S and 30°N. As shown in Fig. 13a, the wave energy input in January was larger in Z1 than in the other zones, and the maximum value was greater than 1.2 W/m^2. The next highest wave energy input in January was found for Z5, for which the maximum value was about 0.4 W/m^2. As shown in Fig. 14a, the wave energy input in July was almost 0 in Z1 and over the whole of the northern Pacific, and it gradually increased while moving south and reached a maximum approaching 1 W/m^2 near 60°S in Z5, in the southern Pacific. Like the wind speed and the signific-

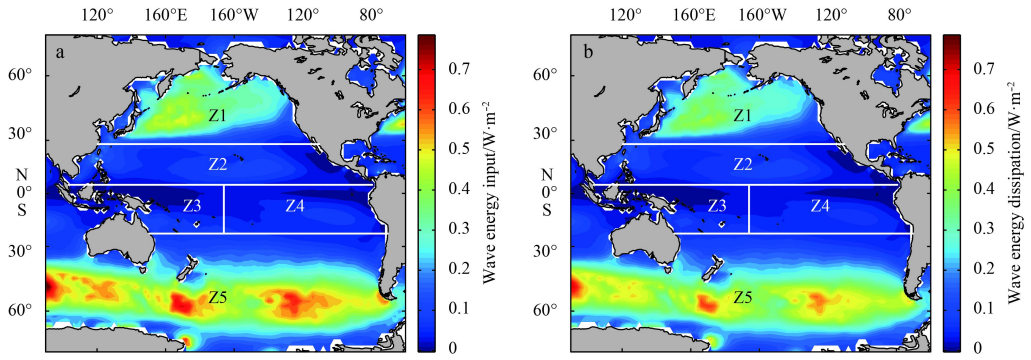

Fig. 12. Ten-year average wave energy input (a) and dissipation (b) distributions for the period 2002–2011.

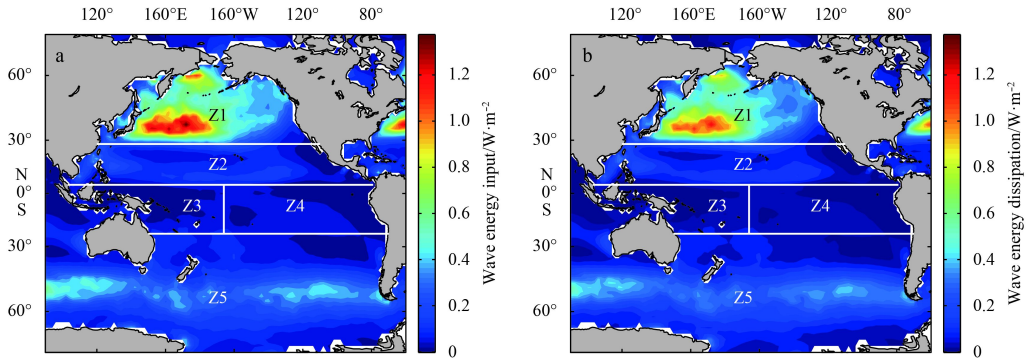

Fig. 13. Ten-year average wave energy input (a) and dissipation (b) for January.

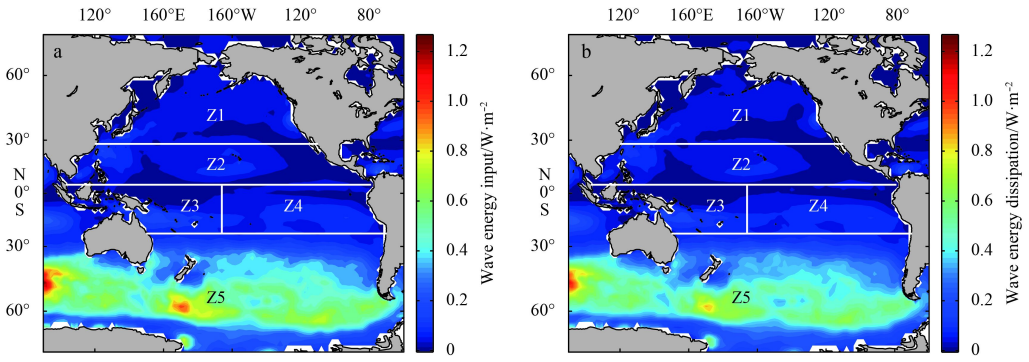

Fig. 14. Ten-year average wave energy input (a) and dissipation (b) for July.

ant wave height, the maximum wave energy input was found in the northern Pacific in January throughout the year. The wave energy inputs in January and July in Z2, Z3, and Z4 were all almost 0, so no clear seasonal variations were found in these areas. The distributions of the wave energy dissipation and input corresponded (see Figs 13b and 14b).

4.4 *Power spectrum analysis*

Time series of daily average wind speeds and significant wave heights for each zone were calculated to allow the temporal evolutions of the wind speed and the significant wave height in each zone to be evaluated. The power spectral density (PSD) was analyzed to show the variations in the wind speed and the significant wave height on different time scales. The estimated power spectra and the standard spectra for the wind speed are shown in Fig. 15. Where the peak of a power spectrum exceeds the peak of the standard spectrum this implies that the corresponding peri-

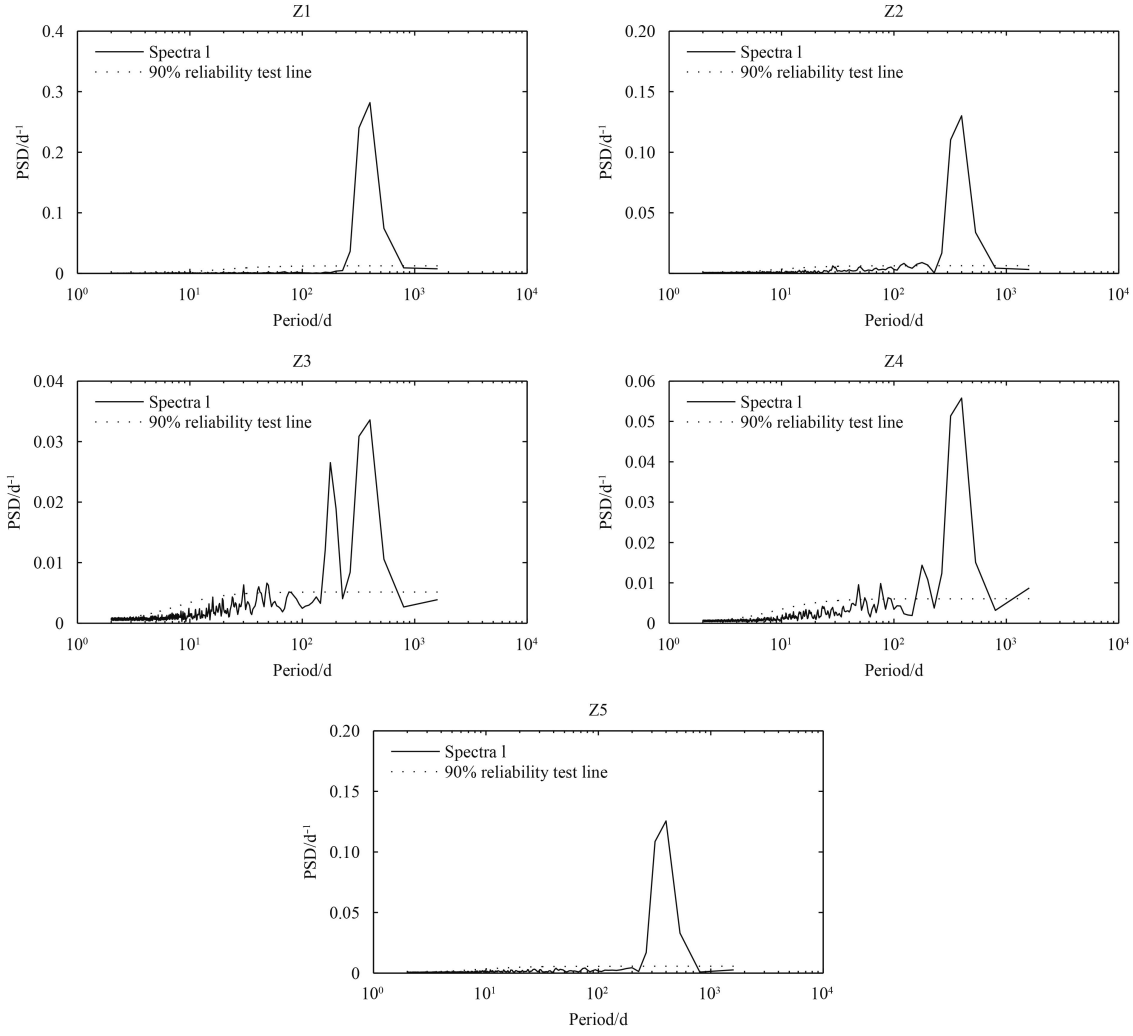

Fig. 15. Spectra of the daily series of wind speed averages for Zones 1–5 of the Pacific Ocean. The dot lines show the 90% reliability levels.

od is significant.

The yearly period was significant in all the zones. No other significant periods were found for Z1 and Z2 in the northern Pacific or Z5 in the southern Pacific in addition to the yearly period. A half-yearly period was almost as significant as the yearly period for Z3, the western part of the equatorial area. In addition, clear intraseasonal oscillation was also found in Z3, and three significant periods were about 30, 40, and 50 d, respectively. The yearly and half-yearly periods and the intraseasonal oscillation were found for Z4, but the half-yearly period oscillation was not as strong in Z4 as in Z3.

The estimated power spectra and standard spectra of the significant wave heights are shown in Fig. 16. There were also relatively large differences between significant periods in the time series of the daily average significant wave heights for all zones.

Similar significant periods to those found for the wind speed time series were found for each zone for the significant wave height series. Only the yearly period was significant for Z1, Z2, and Z5. Unlike for the wind speed series, the half-yearly period was not significant for Z4. However, the other periods that were significant for the wind speed series for Z4 were also significant for the significant wave height series. The results for Z3 were of particular interest because the half-yearly period was still significant and the intraseasonal oscillation still existed but the yearly period was not significant.

The special half-yearly period for Z3 is related to the location of Z3 in the monsoon region north of Australia. Pogarskii et al. (2012) found the wind speed and significant wave height variations with a period of 0.5 a in the northern Indian Ocean. The intraseasonal oscillation we found in the equatorial zones agrees well with a 30–50 d oscillation in a monsoon circulation over East Asia and Australia (Wang and He, 1991).

5 Discussion

By dividing the Pacific Ocean into five zones, and analyzing the wind and wave characteristics in each we obtained the spatial distributions, and temporal variations of, the wind speeds and the significant wave heights in the different zones, showing all the different characteristics. The significant wave height is directly related to the wind speed, so we divided the significant wave height field into five zones using the same zone boundaries as those used for the wind speed field. But actually, considering the existence of swell, the distribution characteristics of the wind speed and the significant wave height do have differences and the waves in one region would have been affected by waves from other regions. The intrusion of swells from high latitudes would

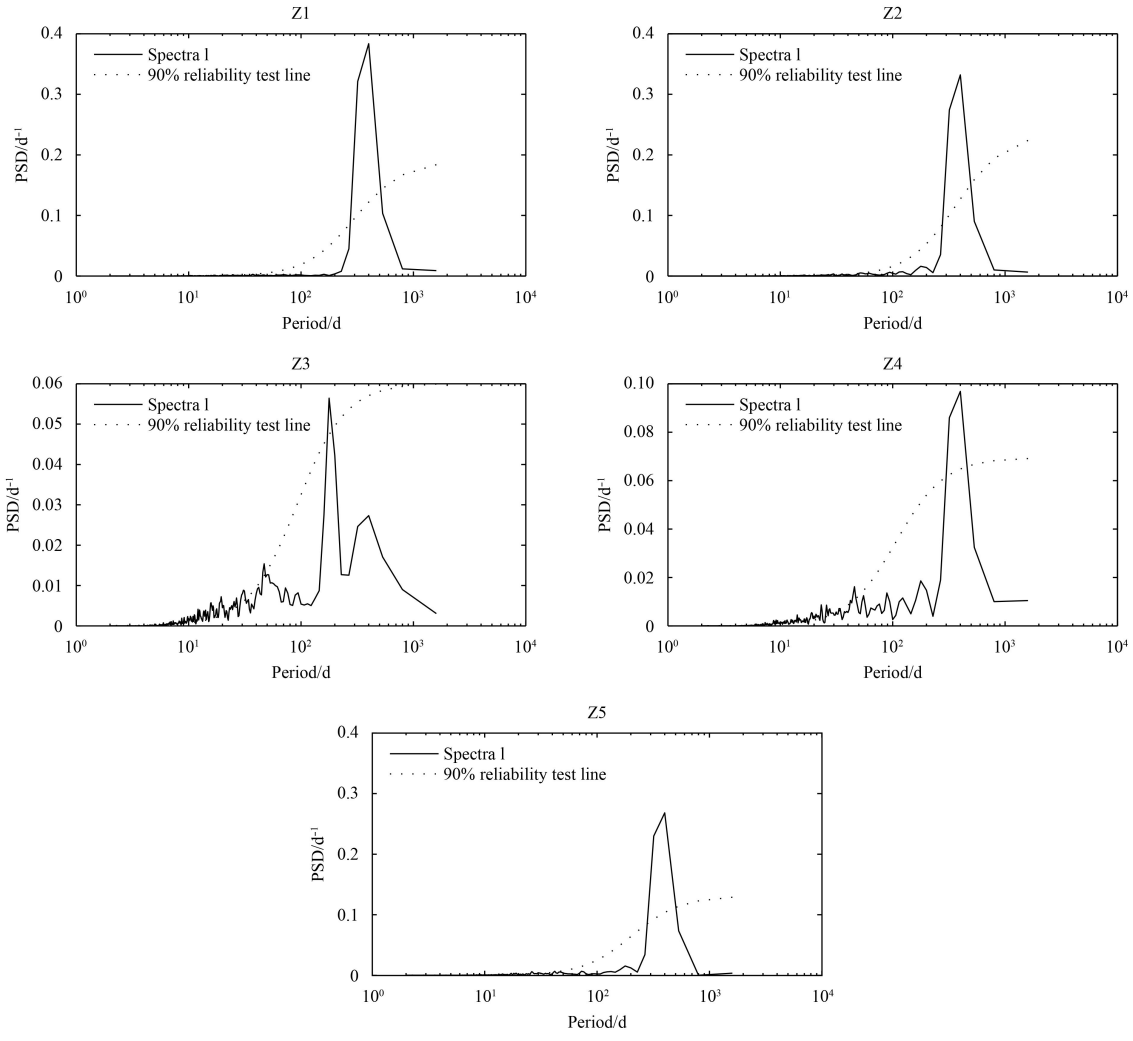

Fig. 16. Spectra of the daily series of significant wave height averages for Zones 1–5 of the Pacific Ocean. The dot lines show the 90% reliability levels.

have resulted in mixed sea states, especially in Z2 and Z4 (Fig. 9). The significant wave height in Z2 in the boreal winter is influenced by high waves in Z1. Swells in Z5 penetrate Z4 in the boreal summer. The overlap between the swell and the local wind-sea introduces nonlinearity between the significant wave height and wind speed statistics. The power spectra and trends in these zones also contain signals from remote areas. Energy of wind-sea and swell should therefore be analyzed separately in these zones. Even in the wind-sea-dominated zones (Z1 and Z5), decay in the wind speed or a change of the wind direction result in swells. It is important to understand these phenomena in order to gain an understanding of the wave distributions, so more elaborate simulations are certainly required. We will assess this matter further in our next paper.

Our numerical simulation results were generally consistent with observations made using buoys, but relatively large differences between the simulation results and the observations were found in the middle of the ocean, near the Hawaiian Islands. The presence of islands may have affected the wind speed or the wave height, but the differences may also have been caused by shortcomings in the ability of the WW3 Tolman and Chalikov package to simulate swells (Bi et al., 2015). We will use the ST6 packages in future simulations to improve the accuracy of the modeling process. This will also facilitate the energy partitioning of wave systems.

6 Conclusions

In terms of statistical averages, the WW3 wave model is effective for hindcasting the significant wave heights in the Pacific Ocean. The correlation coefficient for the relationship between the model results and the buoy data was greater than 0.9, the mean relative bias was 0.09, and the mean RMSE was 0.48 m. The error at mid-latitudes in the northern Pacific was relatively small. The maximum correlation coefficient was 0.97; the mean relative bias was 0.05, and the minimum RMSE was 0.21 m. The error at low latitudes in the northern Pacific was relatively large. The minimum correlation coefficient was 0.90, the mean relative bias was 0.274, and the maximum RMSE was 0.73 m.

We found clear seasonal variations in the significant wave height in the Pacific Ocean. The difference between the significant wave heights in January and July over the 10 a in the study period shows that the largest seasonal variations are at middle and high latitudes of the northern Pacific, where the significant wave height is more than 3 m higher in January than in July. The weakest seasonal variations were found in the equatorial zone, where the seasonal variation was less than 1 m. The wave energy input and dissipation distributions also show clear seasonal variations in the southern and northern Pacific but not between 30°S and 30°N.

Dividing the Pacific Ocean into five zones allowed the characteristics of zonal distributions of the multiyear average wind speeds and significant wave heights to be identified. There were significant differences between the interannual and seasonal variations in the wind speed and the significant wave height in different zones. In general, the modeled significant wave heights increased by an average of 0.56 cm/a during the 10 a study period, but the trends in the annual variations in the significant wave heights in the different zones were very different.

The power spectrum analyses of the wind speeds and the significant wave heights allowed the relationships and differences between the wave field and the forcing field to be investigated in more detail. The wave field recorded seasonal variations and high-frequency variations in the wind speed field, but, at the same time, there were some differences between the variations in the significant wave heights and the wind speeds. Our results suggest that it will be necessary to divide the Pacific Ocean into several zones in future wind–wave studies.

References

Appendini C M, Torres-Freyermuth A, Salles P, et al. 2014. Wave climate and trends for the Gulf of Mexico: a 30-yr wave hindcast. Journal of Climate, 27(4): 1619–1632

Bi Fan. 2013. On the wave-induced effect to circulation transport and the characteristics of swell propagation and dissipation (in Chinese) [dissertation]. Qingdao: Ocean University of China

Bi Fan, Song Jinbao, Wu Kejian, et al. 2015. Evaluation of the simulation capability of the Wavewatch III model for Pacific Ocean wave. Acta Oceanologica Sinica, 34(9): 43–57

Han Shuzong, Zhu Dayong, Guo Peifang. 2003. A study of distribution and variation rules of SWH in the Pacific Ocean by using the satellite altimetry data. Journal of Ocean University of Qingdao (in Chinese), 33(6): 825–832

He Hailun, Chen Dake. 2011. Effects of surface wave breaking on the oceanic boundary layer. Geophysical Research Letters, 38(7): L07604

He Hailun, Xu Yao. 2016. Wind-wave hindcast in the Yellow Sea and the Bohai Sea from the year 1988 to 2002. Acta Oceanologica Sinica, 35(3): 46–53

Kalantzi G D, Gommenginger C, Srokosz M. 2009. Assessing the performance of the dissipation parameterizations in WAVEWATCH III using collocated altimetry data. Journal of Physical Oceanography, 39(11): 2800–2819

Li Shuang, Li Ming, Gerbi G P, et al. 2013. Roles of breaking waves and Langmuir circulation in the surface boundary layer of a coastal ocean. Journal of Geophysical Research: Oceans, 118(10): 5173–5187

Liu Jinfang, Jiang Wei, Yu Mugeng, et al. 2002. An analysis on annual variation of monthly mean sea wave fields in North Pacific Ocean. Journal of Tropical Oceanography, 21(3): 64–69

Longuet-Higgins M S, Stewart R W. 1961. The changes in amplitude of short gravity waves on steady non-uniform currents. Journal of Fluid Mechanics, 10(4): 529–549

Longuet-Higgins M S, Stewart R W. 1962. Radiation stress and mass transport in gravity waves, with application to “surf-beats”. Journal of Fluid Mechanics, 13(4): 481–504

Ma Yawei, Cong Aili, Tian Yanyan, et al. 2013. Statistics analysis of seasonal characteristics of sea surface wind field in the North Pacific Ocean during the last 45 years. Science & Technology Information (in Chinese), (31): 105–111

Mentaschi L, Besio G, Cassola F, et al. 2015. Performance evaluation of WaveWatch III in the Mediterranean Sea. Ocean Modelling, 90: 82–94

Pogarskii F, Polnikov V, Sannasiraj S A. 2012. Joint analysis of the wind and wave-field variability in the Indian Ocean area for 1998–2009. Izvestiya, Atmospheric and Oceanic Physics, 48(6): 639–656

Song Jinbao, Fan Wei, Li Shuang, et al. 2015. Impact of surface waves on the steady near-surface wind profiles over the ocean. Boundary-Layer Meteorology, 155(1): 111–127

Tolman H, Accensi M, Alves H, et al. 2014. User Manual and System Documentation of Wavewatch III Version 4.18. Technical Note 316: NOAA/NWS/NCEP/MMAB, 12–68

Tolman H L, Chalikov D. 1996. Source terms in a third-generation wind wave model. Journal of Physical Oceanography, 26(11): 2497–2518

Wang Jianhong, He Jinhai. 1991. The 30–50 day oscillation characteristic of monsoon circulation over East Asia and Australia during the winter of 1982–1983. Journal of Tropical Meteorology, (2): 104–112

Zhang Peng, Chen Xiaoling, Lu Jianzhong, et al. 2011. Research on wave simulation of Bohai Sea based on the CCMP remotely sensed sea winds. Marine Science Bulletin (in Chinese), 30(3): 266–271

Zhang Hongsheng, Gu Junbo, Wang Hailong, et al. 2013. Simulating wind wave field near the Pearl River estuary with SWAN nested in WAVEWATCH. Journal of Tropical Oceanography (in Chinese), 32(1): 8–17

Zheng Chongwei, Lin Gang, Sun Yan, et al. 2012. Analysis of wave characteristics in the Pacific Ocean during the last 45 years. Journal of Tropical Oceanography, 31(6): 6–12

Zheng Chongwei, Pan Jing, Li Jiaxun. 2013. Assessing the China sea wind energy and wave energy resources from 1988 to 2009. Ocean Engineering, 65: 39–48

Zhou Ke, Zhu Zhixia, Yang Yang. 2009. Simulation of ocean wave in the northwest Pacific Ocean. Journal of Zhejiang University: Science Edition (in Chinese), 36(5): 603–608